New Journal of Physics
The open access journal at the forefront of physics

Deutsche Physikalische Gesellschaft DPG
IOP Institute of Physics

Published in partnership with: Deutsche Physikalische Gesellschaft and the Institute of Physics

OPEN ACCESS

RECEIVED
1 January 2020

REVISED
29 June 2020

ACCEPTED FOR PUBLICATION
6 July 2020

PUBLISHED
4 September 2020

PAPER

Relativistic mid-wavelength infrared pulses generated in intense-laser mass-limited target interactions

J F Qu[1,2], P Liu[1], X Y Liu[1,3], R J Gray[2], P McKenna[2], X F Li[4,5,6,8], S Kawata[7] and Q Kong[1,8]

[1] Key Laboratory of Nuclear Physics and Ion-beam Application (MOE), Institute of Modern Physics, Department of Nuclear Science and Technology, Fudan University, Shanghai, 200433, People's Republic of China
[2] Department of Physics, SUPA, University of Strathclyde, Glasgow, G4 0NG, United Kingdom
[3] Key Laboratory of Pulsed Power, Institute of Fluid Physics, CAEP, Mianyang 621900, People's Republic of China
[4] Key Laboratory for Laser Plasmas (MoE), School of Physics and Astronomy, Shanghai Jiao Tong University, Shanghai 200240, People's Republic of China
[5] Collaborative Innovation Center of IFSA (CICIFSA), Shanghai Jiao Tong University, Shanghai 200240, People's Republic of China
[6] Institute for Advanced Simulation, Jülich Supercomputing Centre, Forschungszentrum Jülich, 52425 Jülich, Germany
[7] Graduate School of Engineering, Utsunomiya University, Utsunomiya 321-8585, Japan
[8] Authors to whom any correspondence should be addressed.

E-mail: qkong@fudan.edu.cn and xiaofengli@sjtu.edu.cn

Keywords: mid-wavelength infrared radiation, mass-limited target, relativistic laser, plasma

Supplementary material for this article is available online

Abstract

Infrared spectroscopy, ultra-fast x-ray high harmonic generation, and time-resolved imaging of molecular structures benefit from the availability of intense mid-infrared wavelength pulses. Here we present a new approach to generating these, in which an intense short laser pulse is incident upon a near-critical density, spherical, mass-limited carbon target. After the laser pulse interaction, the carbon ions produced form a central force field. Plasma electrons accelerated by the laser return to the positively charged carbon target under the action of this field. The energy of these electrons is reduced and is lower than their energy in the laser field. These low-energy refluxing electrons start to oscillate with a rotating figure-of-eight motion around the positively charged carbon target and emit relativistically intense mid-infrared pulses with the wavelength in the range 1 to 4 μm.

1. Introduction

Significant progress has been made in obtaining high-quality mid-wavelength infrared (MWIR) sources in recent decades, which has opened new avenues of research in the field of laser-matter interactions. These high-quality sources are important for a broad range of applications in ultrafast physics, chemistry, biology and materials science, including infrared spectroscopy [1], ultra-fast x-ray high harmonic generation [2, 3], time-resolved imaging of molecular structures [4, 5], attosecond pulse radiation [6] and filamentation [7]. Short pulse MWIR generation is, however, one of the challenges for ultra-fast laser technology. Traditionally, laser-based infrared pulse generation depends on optical parametric amplifiers pumped by lasers operating at 1 μm [8, 9], optical parametric chirped-pulse amplifiers in $ZnGeP_2$ crystals [10, 11] and CO_2 lasers [12, 13], which typically produce wavelengths beyond 5 μm due to a lack of nonlinear crystals with suitable optical and mechanical properties. Other infrared generation methods, such as difference frequency generation [14], adiabatic difference generation [15], non-degenerate four-wave-mixing [16] and optical rectification [17], have also been explored. These schemes involve nonlinear crystals that have the energy-density damage threshold limitations for laser pulse power/intensity scaling. This problem is inherently avoided by the use of plasma as the frequency conversion medium. Recently, for example, it has been demonstrated that infrared pulses with wavelength from 5 to 14 μm can be obtained by utilizing

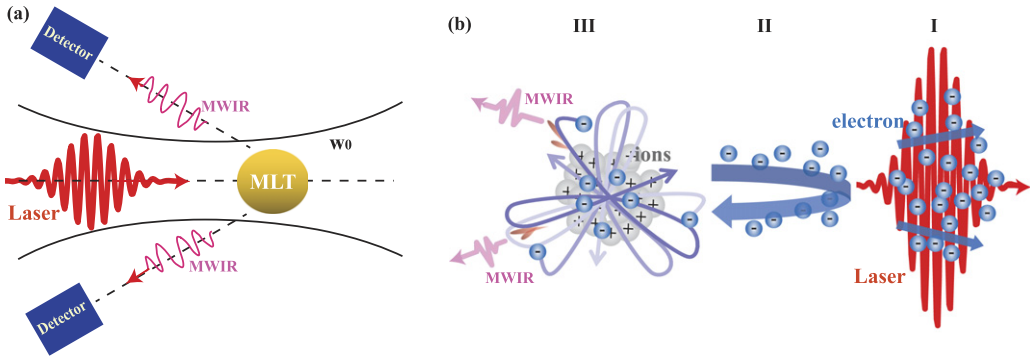

Figure 1. (a) Schematic diagram of the laser-MLT interaction geometry. (b) The steps in the MWIR generation process: I. Electrons driven forward by the laser light; II. Electrons reflected back by the positive charge; III. Electrons refluxing about the positively charged ions to emit MWIR radiation outwards.

asymmetric self-phase modulation produced by a wake in a tailored plasma density structure, such that the pump laser pulse continuously downshifts in frequency [18]. Theory and numerical studies have been used to investigate the compression of a high power laser pulse to the order of the laser wavelength in plasma [19] and pulse energy depletion and spectral shifts produced by large amplitude plasma waves [20]. These processes result in the production of a strong mid-infrared pulse. Aside from plasma, high energy electron beams have been shown to be a potential medium for the generation of mid-infrared pulses. A pump electron beam is injected into a seed terahertz pulse, amplifying the field of the seed pulse and upshifting the central wavelength to mid-infrared range [21].

The MWIR pulse generation research referenced above focuses on pulse compression and frequency shifting. Another common method is to utilize the dynamics of collective acceleration and deceleration of charged particles to emit electromagnetic waves in ultra-intense laser-plasma interactions. In the target normal sheath acceleration regime for the acceleration of ions, energetic electrons generated by the laser pulse at the target front side travel through the target and emerge at the rear side, generating a plasma sheath with associated electrostatic field [22]. Under the action of the sheath field, the energetic electrons experience acceleration and deceleration, and thereby emit electromagnetic radiation [23]. The use of a mass-limited target (MLT) has been explored in theoretical [24, 25] and experimental [26, 27] studies. The dimensions of an MLT can be less than, or comparable to, the laser spot size, enabling the whole target to be pushed forward by the laser radiation pressure and for a large fraction of the electrons to be accelerated. The electron oscillatory and recirculation motions are restricted transversely by the laser transverse ponderomotive force, resulting in a strong longitudinal charge separation. When the laser intensity is high enough, the kinetic energy of the electrons increase in the longitudinal direction [28] and ions [29] can be directly accelerated longitudinally, together with the electrons. These accelerated particles emit ultrabright x-rays [30] in the radiation pressure acceleration regime [31]. Thus, MLTs are often used as a pulsed source of electromagnetic waves with high frequency, such as gamma ray [32] and EUV [33] radiation. In the limit in which the laser intensity is not high enough to directly accelerate ions, and the charge separation field does not accelerate ions, a portion of the electron population is pulled back towards the positively charged ions. These electrons lose energy and reflux about the positively charged target. Their collective refluxing motion can drive the production of low frequency radiation.

2. Simulation and discussion

This article introduces a novel method for the generation of mid-infrared pulses that utilizes the interaction of refluxing electrons and the positively charged ions in an MLT. When a relativistically intense, short laser pulse exerts radiation pressure on a near-critical-density, spherical, carbon MLT, almost all of the electrons are displaced resulting in a strong charge separation field. The positively charged carbon ions left behind start to experience Coulomb explosion (CE) [34, 35] and form a central force field. Part of the electron population is attracted back towards the ions. The electrons overshoot the central potential and, under the action of the central force field, oscillate about the carbon ions with a rotating figure-of-eight motion. This collective motion forms a periodicity rotating current macroscopically and results in the emission of mid-infrared electromagnetic radiation in the wavelength range from 1 to 4 μm. Figure 1 shows schematic diagrams of the laser-MLT interaction geometry and the three stages of the MWIR generation process.

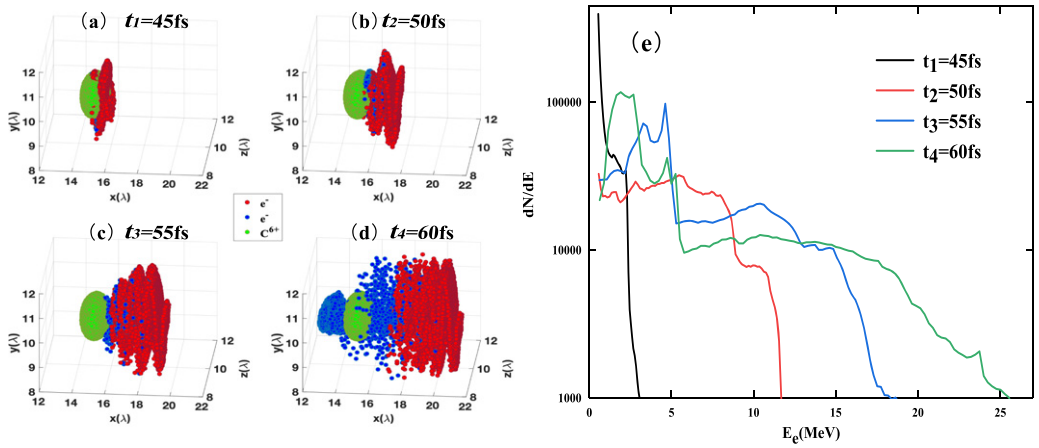

Figure 2. An intense, short laser pulse interacts with a mass-limited, spherical carbon plasma (a)–(d): the distribution evolution of the electrons and carbon ions at (a)$t_1 = 45$ fs, (b)$t_2 = 50$ fs, (c)$t_3 = 55$ fs and (d)$t_4 = 60$ fs, where the refluxing electrons are marked by blue dots and the forward-directed electrons are marked by red dots. (e) The corresponding energy spectra of the refluxing electrons at the same four sample times.

The MWIR generation is attributed to the periodic acceleration and deceleration of refluxing electrons under the action of the central force. Normally, the magnitude of the central force field is only related to the displacement of a particle with respect to the centre and is expressed as follows (according to Gauss' theorem): $\vec{E_r} = \frac{Q(R_0)}{4\pi\epsilon_0} r^n \widehat{E}$. Here Q is the total positive charge, R_0 is the initial radius of the charged particle and r is the distance from the particle to centre. The trajectory of a particle with a given energy and momentum, subject to the central force, can be accurately calculated. It is found that a large number of the trajectories are non-closed orbits [36]. Each orbit has many apogees, perigees and turning points. This phenomenon occurs for different central fields, in which n differs, or an extra magnetic field is added [37]. This provides the conditions for the acceleration and deceleration of the particle. In the following, the electron trajectories are calculated using the Runge–Kutta method to solve the above formula.

The three-dimensional particle-in-cell (PIC) code EPOCH [38] was used to simulate the interaction of an ultra-intense laser pulse with a near-critical-density carbon MLT, including the interactions between the refluxing electrons and carbon ions. The simulation box was $x \times y \times z = 30\lambda_0 \times 20\lambda_0 \times 20\lambda_0$, with spatial mesh equal to $3000 \times 640 \times 640$. Each cell had 32 macro-particles. A linearly polarized Gaussian laser pulse with dimensionless peak amplitude $a_0 = 20$ (where a_0 is related to the laser intensity, I, through the relation $I = 1.37 \times 10^{18} a_0^2$ [Wcm^{-2}]$/\lambda_0^2$ [μm]) was incident in the x-direction from the left side of the simulation box to irradiate the MLT. The laser wavelength $\lambda_0 = 0.8\,\mu$m, pulse duration $\tau = 10$ fs and the focal waist $w_0 = 5\lambda_0$. The target was a uniform spherical carbon plasma with radius $R_0 = 0.8\lambda_0$ (which is smaller than the laser spot size), with the centre located at $[x = 15\lambda_0, y = 10\lambda_0, z = 10\lambda_0]$. The initial, uniform electron density $n_e = 0.6 n_c$, where $n_c = m_e \epsilon_0 \omega_0^2 / e^2$ is the critical plasma density (i.e. the density above which laser light of a given wavelength cannot propagate).

Figure 2 shows the typical distribution evolution of the carbon ions (green) and electrons (forward-directed electrons in red and refluxing electrons in blue), and the energy spectra distribution of the refluxing electrons at stated times. There are several characteristic stages to the electron dynamics during the interaction. At $t = 40$ fs, the laser pulse starts irradiating the carbon target. The outer wings of laser pulse continue to propagate and envelop the whole target. Almost all electrons are instantly accelerated forward in response to the laser pulse and a charge separation field forms between $t_1 = 45$ fs and $t_2 = 50$ fs. The energy of the electrons involved in refluxing increases to a peak value of ~6 MeV, as determined by the electron ponderomotive energy $(\sqrt{1 + a_0^2/2} - 1) m_e c^2 = 6.75$ MeV. The relatively immobile carbon ions produce a strong central force field. The electrons that are located at the tail of the forward moving electron cloud feel the combined potential of the central force field and the charge-separation field at the tail of the laser pulse. Under the influence of these fields, this part of the moving electron population (now of the order of a few microns away from the mass-limited target) is attracted back towards the positively charged carbon ions. The energy of these refluxing electrons is reduced, at around $t_3 = 55$ fs. The last of the refluxing electrons start to oscillate around the carbon ions at about $t_4 = 60$ fs. Beyond this time, the refluxing electrons couple in oscillation with the carbon ions undergoing Coulomb explosion under the action of the central force field. This will be described in detail later.

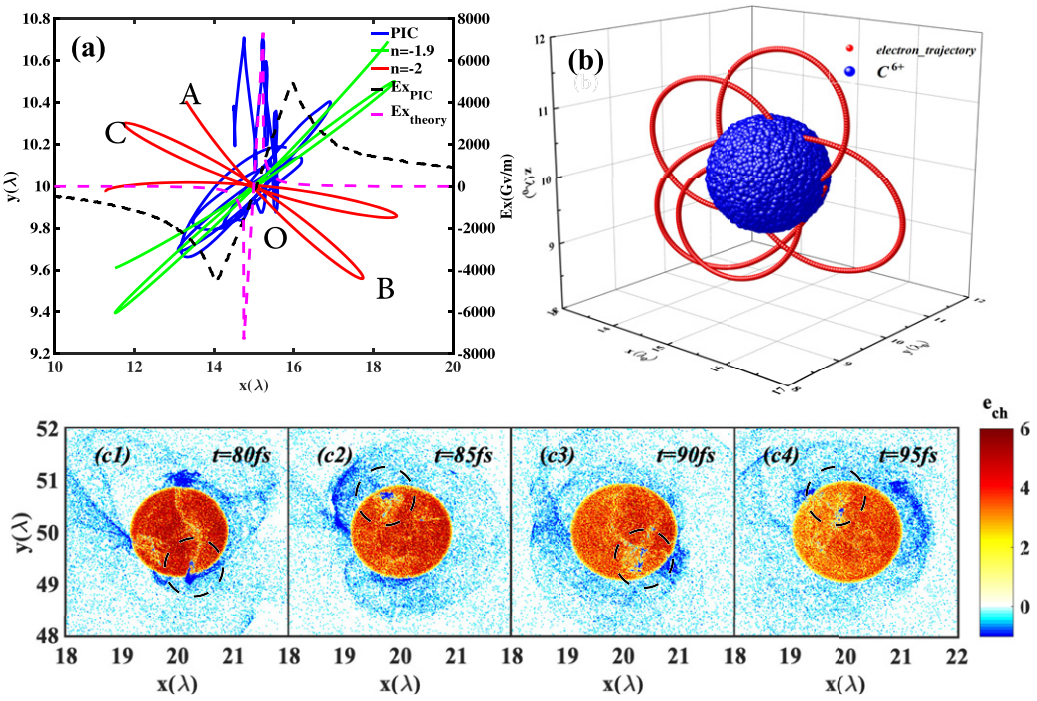

Figure 3. (a) Projection of the motion of an electron in the *XY* plane for different initial position and velocity, and different n, using the Runge–Kutta method (red and green) and from PIC simulation (blue). The electric field distribution from the PIC simulation (black) and from theory (pink) are also shown. (b) The trajectory of an example electron oscillating about the central force field produced by the carbon ions. (c) Projection of the charge density in the *XY* plane at (1)$t_1 = 80$ fs, (2)$t_2 = 85$ fs, (3)$t_3 = 90$ fs and (4)$t_4 = 95$ fs, where the highly negative charge density region is marked by the black dashed circle.

The trajectory of an electron that enters the central force field depends on its initial energy, momentum and incident angle [29]. Figure 3(a) shows a projection of trajectories in the *XY* plane (marked by the solid line) of electrons with different initial energy and momentum, in different central force fields. A typical electron, in the central force field with $n = -2$, firstly experiences acceleration (from A to O), passes the centre of the force (O) and decelerates (from O to B) until it turns (point B). The electron thus oscillates back and forth due to the central force field. Moreover, because the electron is injected at an angle, its trajectory also rotates or precesses (from A to B to C). As shown in figure 3(a), for central force fields with different n ($=-2$ or -1.9 in the examples shown), the electrons dynamics are similar. In other words, the electron motion in a central force field has two components: an oscillatory back and forth motion, and a precession. The combined effect is similar to a rotating figure-of-eight motion.

The central force field (generated by the positively charged carbon ions) in the PIC simulation is shown in figure 3(a) by the dashed black line and exhibits two features: one is a linear change region inside the target and the other is a rapid decrease in field strength with increasing radius outside the target. The separation between the two peaks in the field is the diameter of the spherical target comprising of the carbon ions. This distance is larger than that predicted by theory, as shown by the dashed pink line. The separation of the peaks continues to increase with time in the PIC simulation because the positively charged carbon ionic core also experiences CE. In fact, due to the presence of the refluxing electrons the rate of increase is much lower than would be expected for CE of the ion core in the absence of electrons. Thus, the interaction between the refluxing electrons and positively charged ions occurs over a time frame of about 70 fs and then the expected CE begins, as shown in the supplementary information (https://stacks.iop.org/NJP/22/093007/mmedia). Figure 3(b) shows a 3D simulation of the trajectory of a refluxing electron about the positively charged central force field. The trajectory projection of the same electron, in the *XY* plane, is shown in figure 3(a) as the solid blue line. It is seen that an electron firstly experiences transverse oscillation along the propagation axis, as defined by the laser pulse. Then it is pulled back towards the carbon ion target and oscillates with the rotating figure-of-eight shape in the central force field, as shown in figure 3(b). Because the energy of the refluxing electron interacting with the positively charged carbon ions is much lower than the kinetic energy acquired in the laser field [39], the electron oscillation frequency is slower than that in the laser field. The frequency of the generated radiation can therefore also be lower than laser frequency.

In the PIC simulations, up to 85% of the refluxing electrons make this figure-of-eight trajectory. Macroscopically, electrons with similar trajectories form a rotating current around the positively charged

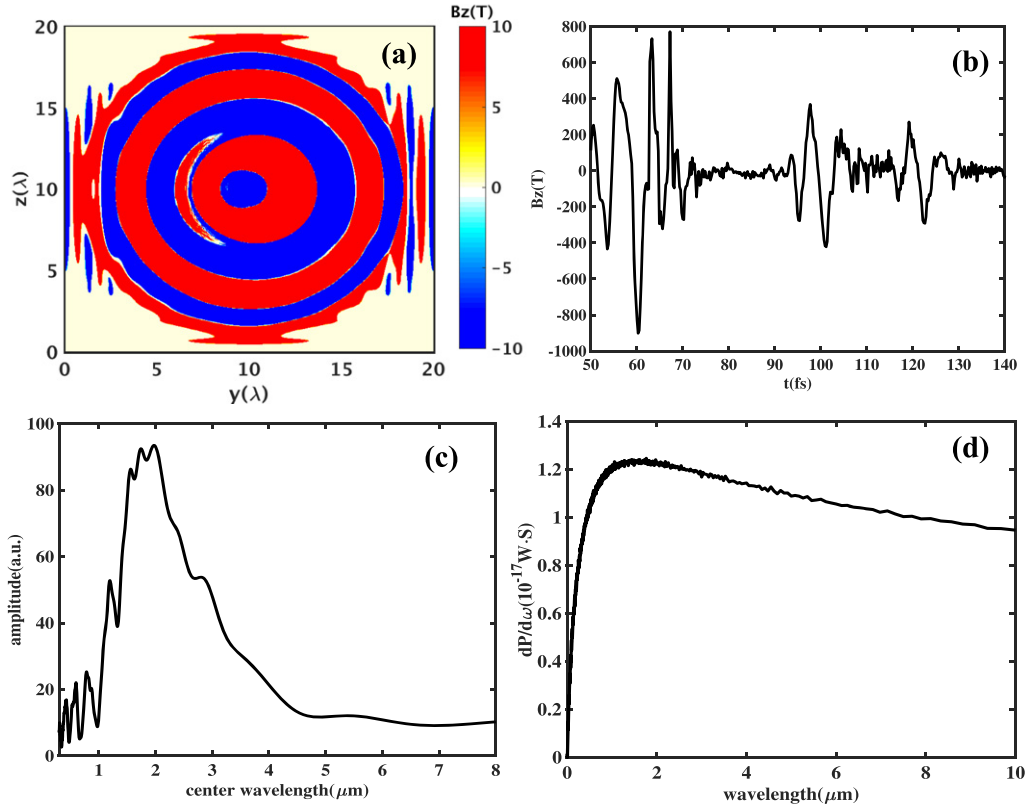

Figure 4. (a) Spatial distribution of the magnetic field in the *YZ* plane at $x = 10\lambda_0$. (b) Temporal magnetic field waveform at point $[x = 10\lambda_0, y = 10\lambda_0, z = 10\lambda_0]$. (c) Corresponding Fourier frequency spectrum. (d) The synchrotron radiation produced by the single electron of figure 3(b).

carbon ions target, as shown in figure 3(c). The charge density distribution is thus composed of two parts: the electron cloud outside the target and the non-uniform charge density distribution inside the target. The former is caused by a population of refluxing electrons that move outside the target to form an electron cloud. Other refluxing electrons enter the area inside the target and neutralize the positively carbon charged ions, locally reducing the positive charge density. The black dotted circle in figure 3(c) represents a highly negative charge density region. The collective motion of the electrons in this negative charge density region and the electrons cloud appears periodic and rotates counterclockwise, from $t = 80$ fs to $t = 95$ fs. Macroscopically, the periodically rotating current generates unique synchrotron electromagnetic radiation.

The simulation results in figures 4(a)–(d) show the electromagnetic radiation produced in the laser-MLT interaction. Figure 4(a) shows the spatial distribution of the magnetic field *Bz*, sampled in the vacuum ($x = 10\lambda_0$) at $t = 65$ fs. The electromagnetic radiation is emitted from the target within a cone angle, presenting a ring-shape distribution in the *YZ* plane. The wavelength corresponding to one cycle of the ring-shaped magnetic field is longer than the laser wavelength. Figure 4(b) presents the temporal evolution of *Bz* at a fixed point ($y = 10\lambda_0, z = 10\lambda_0$) located at the centre of the circle in figure 4(a). The evolution time frame is about 70 fs, consistent with the time frame of interaction between the refluxing electrons and positively charged ions. After filtering the noise, the corresponding Fourier frequency spectrum is presented in figure 4(c) and has a central peak value at around ~ 2 μm and a wide range from 1 to 4 μm. This result is consistent with the synchrotron radiation of the single electron in figure 3(b) and is presented in figure 4(d). It is the first numerical simulation to demonstrate mid-infrared pulse generation in the interaction of refluxing electrons under the action of a central force field.

Through the comparison of 2D and 3D PIC simulations, it is found that the characteristics of radiation generated are similar, and especially the central wavelength, as shown in the supplementary information. Due to computing limitations, 2D simulations are used for parametric investigation of the dependence of the radiation properties on the laser-plasma. With the exceptions of the variables a_0, n_p and R_0, all other laser parameters are the same as those of the above 3D simulation. The 2D simulation box has dimensions of $100\lambda_0 \times 100\lambda_0$ with $10\,000 \times 10\,000$ cells in x and y directions, respectively. Each cell has 8 macro-particles. The x axis is defined to be the laser pulse propagation direction and the y axis is the laser pulse linear polarization direction. The energy and frequency spectrum of MWIR are detected at $10\lambda_0$ away from the centre of the MLT. Figure 5(a) presents the effects of drive laser intensity on the energy conversion

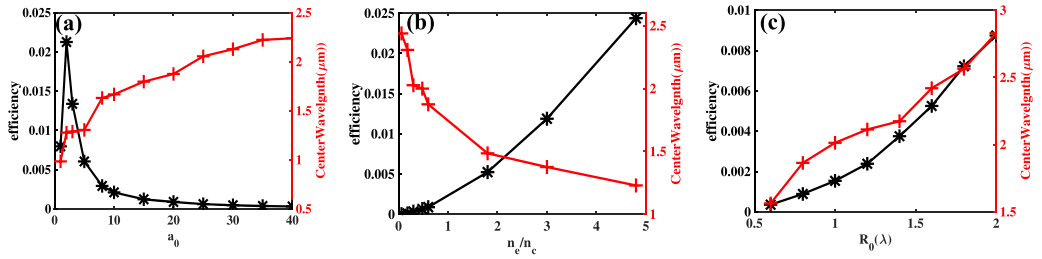

Figure 5. Dependence of energy conversion efficiency and MWIR central wavelength on: (a) laser intensity (in light amplitude units); (b) initial electron plasma density (normalised to the critical electron density); and (c) initial target radius. The electron plasma density is $n_e = 0.6n_c$ in (a) and (c). The dimensionless amplitude of the laser light is $a_0 = 20$ in (b) and (c). The initial target radius is $0.8\lambda_0$ in (a) and (b).

efficiency and central wavelength of the MWIR generated. Note that the maximum value of the energy conversion efficiency appears when the laser intensity is at an optimum value of $a_0 = 3$. This is because when a laser pulse with lower intensity interacts with the MLT, fewer electrons are accelerated, the number of refluxing electrons is lower and the central force field is difficult to form, resulting in inefficient radiation generation. With increasing laser intensity ($a_0 > 10$), an increasing number of electrons are accelerated to high energies by the laser ponderomotive force and, as a result, the number of refluxing electrons decreases, reducing energy conversion efficiency to radiation. The energy of the refluxing electrons increases with increasing laser intensity, which causes the radius of the refluxing electron population to increase, which in turn means that the central wavelength of the emitted radiation increases.

In figure 5(b), the effects of initial plasma density on MWIR radiation generation are considered. The energy conversion efficiency increases with the initial plasma density. The increase in plasma density can bring about an increase in the number of refluxing electrons and the radiation energy therefore increases. The energy conversion efficiency of the mid-IR pulse can be up to 2% when the electron density is $5n_c$. The central wavelength of the radiation is inversely proportional to the plasma density. This observation is explained by the fact that the central wavelength is positively correlated to the plasma wavelength of the refluxing electrons, which is inversely proportional to plasma density. In addition, enlarging the target radius also increases the number of refluxing electrons, further enhancing the radiation energy generated by the refluxing electrons, as shown in figure 5(c). Increasing the target radius also causes the oscillation period of the electrons refluxing around the positively charged ions to increase. As a result, the central wavelength of the radiation emitted becomes longer. In summary, the central wavelength is mainly determined by the oscillation period of the refluxing electrons around the carbon ions, whilst the energy conversion efficiency is mainly determined by the number of refluxing electrons, when other parameters are fixed.

To simplify the model and investigate the physics of the radiation generation mechanism, an initially uniform density sphere is considered above. We also explored the use of different shapes of MLTs, namely an ellipsoid and cylinder, and find that the fundamental properties of the electron dynamics are similar and the MWIR pulse is produced in all these cases. In addition, we consider the role of plasma pre-expansion as is likely to occur in experiment. A spherical target with a linear up-ramp density at the boundary and uniform density distribution in the centre was used. The mid-IR pulses are still obtained when the density scale-length of the up-ramp is twice as large as the radius of the uniform target, as shown in the supplementary information.

3. Conclusion

In conclusion, a numerical study is reported in which mid-infrared pulses are observed for the first time in the interaction of a relativistically strong laser pulse and an MLT. 3D PIC simulation results show that after the laser pulse passes the MLT, a large fraction of the accelerated electrons are pulled back towards the positively charged ion target by the central force field. These refluxing electrons oscillate with a rotating figure-of-eight motion, form a periodically rotating current and emit mid-infrared radiation with central wavelength from 1 to 4 μm. The properties of the MWIR radiation pulse can be changed by variation of the initial laser and target parameters. The mass-limited target structure may prove to be a practical device for generating mid-wavelength infrared pulses in the future.

Acknowledgments

This work was partly supported by NSFC (No. 11775056), China Postdoctoral Science Foundation (No. 2018M641993), China Scholarship Council, JSPS (Japan Society of the Promotion of Science)/MEXT (Ministry of Education, Culture, Sports, Science and Technology).

ORCID iDs

P McKenna https://orcid.org/0000-0001-8061-7091
Q Kong https://orcid.org/0000-0001-7476-8571

References

[1] Calabrese C, Stingel A M, Shen L and Petersen P B 2012 *Opt. Lett.* **37** 2265–7
[2] Popmintchev T *et al* 2012 *Science* **336** 1287–91
[3] Weisshaupt J, Juve V, Holtz M, Ku S, Woerner M, Elsaesser T, Alisauskas S, Pugzlys A and Baltuska A 2014 *Nat. Photon.* **8** 927–30
[4] Blaga C I, Xu J, DiChiara A D, Sistrunk E, Zhang K, Afostini P, Miller T A, DiMauro L F and Lin C D 2012 *Nature* **483** 194–7
[5] Koch M, Symvoulidis P and Ntziachristos V 2018 *Nat. Photon.* **12** 505–15
[6] Hernandez-Garcia C, Perez-Hernandez J A, Popmintchev T, Murnane M M, Kapteyn H C, Jaron-Becker A, Becker A and Plaja L 2013 *Phys. Rev. Lett.* **111** 033002
[7] Silva F, Austin D R, Thai A, Baudisch M, Hemmer M, Faccio D, Couairon A and Biegert J 2012 *Nat. Commun.* **483** 194–7
[8] Andriukaitis G, Balciunas T, Alisauskas S, Pugzlys A, Baltuska A, Popmintchev T, Chen M C, Murnane M M and Kapteyn H C 2011 *Opt. Lett.* **36** 2755–7
[9] Zhao K, Zhong H, Yuan P, Xie G, Wang J, Ma J and Qian L 2013 *Opt. Lett.* **38** 2159–61
[10] Grafenstein L, Bock M, Ueberschaer D, Zawilski K, Schunemann P, Griebner U and Elsaesser T 2017 *Opt. Lett.* **42** 3796–9
[11] Sanchez D, Hemmer M, Baudisch M, Cousin S L, Zawilski K, Schunemann P, Chalus O, Simon-Boisson C and Biegert J 2016 *Optica* **3** 147–50
[12] Haberberger D, Tochitsky S and Joshi C 2010 *Opt. Express* **18** 17865–75
[13] Polyanskiy M N, Pogorelsky I V and Yakimenko V 2011 *Opt. Express* **19** 7717–25
[14] Pupeza I *et al* 2015 *Nat. Photon.* **9** 721–5
[15] Krogen P, Suchowski H, Liang H, Flemens N, Hong K H, Kartner F X and Moses J 2017 *Nat. Photon.* **11** 3246–9
[16] Nomura Y, Shirai H, Ishii K, Tsurumachi N, Voronin A A, Zheltikov A M and Fuji T 2012 *Opt. Express* **20** 24741–7
[17] Pigeon J J, Tochitsky A Y, Gong C and Joshi C 2014 *Opt. Lett.* **39** 3246–9
[18] Nie Z *et al* 2018 *Nat. Photon.* **12** 489–94
[19] Wilson T C, Li F Y, Weng S M, Chen M, Mckenna P and Sheng Z M 2019 *J. Phys. B: At. Mol. Opt. Phys.* **52** 055403
[20] Zhu W, Palastro P J and Antonsen T M 2013 *Phys. Plasmas* **20** 073103
[21] Thiele I, Siminos E and Fulop T 2019 *Phys. Rev. Lett.* **122** 104803
[22] Wilks S C *et al* 2001 *Phys. Plasmas* **8** 542
[23] Gopal A *et al* 2012 *New J. Phys.* **14** 083012
[24] Psikal J, Limpouch J, Kawata S and Andreev A A 2006 *Czech. J. Phys.* **56** B515
[25] Kluge T, Enghardt W, Kraft S D, Schramm U, Zeil K, Cowan T E and Bussmann M 2010 *Phys. Plasmas* **17** 123103
[26] Henig A *et al* 2009 *Phys. Rev. Lett.* **102** 095002
[27] Sokollik T, Paasch-Colberg T, Gorling K, Eichmann U, Scnurer M, Steinke S, Nickles P V, Andreev A and Sandner W 2010 *New J. Phys.* **12** 113013
[28] Liseykina T V, Pirner S and Bauer D 2010 *Phys. Rev. Lett.* **104** 095002
[29] Matsui R, Fukuda Y and Kishimoto Y 2019 *Phys. Rev. Lett.* **122** 014804
[30] Yu T P, Pukhov A, Sheng Z M, Liu F and Shvets G 2013 *Phys. Rev. Lett.* **110** 045001
[31] Pegoraro F and Bulanov S V 2007 *Phys. Rev. Lett.* **99** 065002
[32] Hu L X, Yu T P, Li H Z, Yin Y, McKenna P and Shao F Q 2016 *Opt. Lett.* **43** 2615
[33] Fujioka S *et al* 2005 *Appl. Phys. Lett.* **87** 241503
[34] Kaplan A E, Dubetsky B Y and Shkolnikov P L 2003 *Phys. Rev. Lett.* **91** 143401
[35] Smirnov M B and Becker W 2004 *Phys. Rev.* A **69** 013201
[36] Hooverman R H 1963 *J. Appl. Phys.* **34** 3505
[37] Johnson C E 1984 *J. Appl. Phys.* **55** 3207
[38] Arber T D *et al* 2015 *Plasma Phys. Control. Fusion* **57** 113001
[39] Bychenkov V Y and Kovalev V F 2005 *Plasma Phys. Rep.* **31** 178–83